ChemComm

Accepted Manuscript

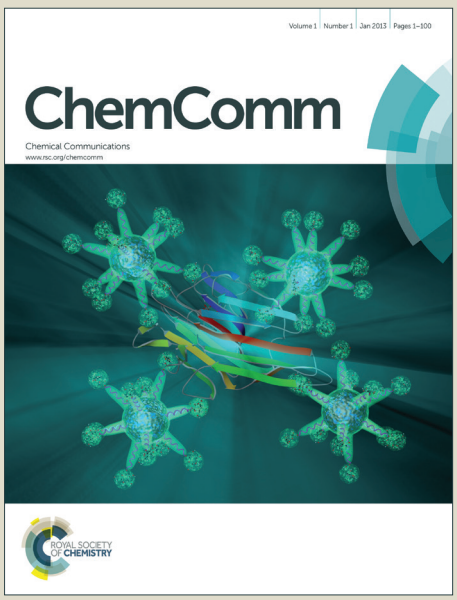

ROYAL SOCIETY OF CHEMISTRY

www.rsc.org/chemcomm

Cite this: DOI: 10.1039/c0xx00000x

www.rsc.org/xxxxxx

ARTICLE TYPE

A highly selective fluorescent probe for cadmium ion in aqueous solution and living cells†

Qiaoling Liu,[a,b] Lixia Feng,[a,b] Caixia Yuan,[a] Lin Zhang,[a] Shaomin Shuang,[a] Chuan Dong,*[a] Qin Hu[c] and Martin M. F. Choi*[c]

Received (in XXX, XXX) Xth XXXXXXXXX 20XX, Accepted Xth XXXXXXXXX 20XX

DOI: 10.1039/b000000x

An organic salt based on double 1,3,4-oxadiazole derivatives as fluorophores and BAPTA as an receptor has been designed for detection of Cd^{2+}. The fluorescent probe exhibits high selectivity for Cd^{2+} and a low detection limit of 20 nM in aqueous solution, making it possible for Cd^{2+} imaging in living MCF-7 cells.

Cadmium (Cd), one of the very important metallic elements, is extensively used in many areas such as metallurgy, electroplating, war industry, nickel-cadmium batteries, pigments, semiconducting quantum dots and rods.[1] The extensive use of Cd leads to serious environmental and health problems including lung, prostatic, and renal cancers.[2] The carcinogenic effect of Cd exposure on laboratory rats showed that between 0.0 and 2.5 μM of $CdCl_2$ could induce tumour incidence and multiplicity; a dose of 2.5 μM could significantly elevate the prostatic tumour incidence; and 20 or 40 μM dosage would strongly induce Leydig cell tumour incidence.[3a] Moreover, Cd can accumulate in human body and cause renal dysfunction, calcium metabolism disorders and other relevant forms of diseases. In 1940s, the Itai-Itai disease in Japan is a typical example.[3] Thus, there is a great demand of developing a facile method with high sensitivity and good selectivity to monitor Cd in environment and biological samples.

Fluorescent probes based on metal ion induced changes in fluorescence appear particular advantages owing to their simple operation and low detection limit. Cadmium ion (Cd^{2+}) probes of different detection mechanisms such as photoinduced electron transfer,[4] intramolecular charge transfer (ICT),[5] chelation-enhanced fluorescence,[6] metal-ligand charge transfer,[7] excimer/exciplex formation,[8] intermolecular hydrogen bonding,[9] and fluorescence resonance energy transfer[10] have been developed. Unfortunately, most of them suffer from UV excitation,[5,8,11] poor water-solubility[11,12] or poor selectivity between Cd^{2+} and Zn^{2+}.[13] Recently several water-soluble Cd^{2+} probes have been introduced but their performances are still far from satisfactory. For instances, there is a relatively small Stokes shift (20 nm) for the Cd^{2+} sensor,[4] or the detection limit is higher than the level of the maximum limit in water stipulated by the US EPA and WHO (4–40 nM).[14] As such, it is highly desirable to develop a new Cd^{2+} probe with better performance in sensitivity and selectivity in aqueous environment.

To our knowledge, fluorescent ICT-based probes have been widely exploited for detection of cations owing to their strong emission intensity and large Stokes shift. These attributes arise from the π-electron conjugation system between the electron donor and electron acceptor, facilitating the ICT process. Once the ICT-based probe has coordinated with metal ions, the ICT is inhibited or reduced with concomitant changes in not only the energy gap between the lowest unoccupied molecular orbital (LUMO) and highest occupied molecular orbital (HOMO) but also the absorption and fluorescence intensity and spectral shifts.[15] So far there are only a few Cd^{2+} probes incorporating the ICT concept. Herein we first report a highly selective and sensitive probe for Cd^{2+} detection based on a novel bichromophoric and bifluorophoric molecule (OBO) and the ICT processes.

The Cd^{2+} probe (OBO) was designed by incorporating a multifunctional ionophore 1,2-bis(2-aminophenoxy)ethane-*N*,*N*,*N*′,*N*′-tetraacetic acid (BAPTA) as the Cd^{2+} receptor with two 1,3,4-oxadiazole derivatives (OXD) to form a sandwich compound OXD-BAPTA-OXD possessing an ICT capability. First, OXD was chosen as the bichromophore and bifluorophore owing to its large Stokes shift and high fluorescence quantum yield. Second, BAPTA is well known for its high selectivity to various metal ions. Third, OBO is a water-soluble salt which can completely dissolve in water to selectively bind with Cd^{2+} in aqueous and cellular environment. Another major attribute of OBO is that it does not respond to most divalent metal ions under visible light excitation.

The detailed synthetic routes and confirmation of the chemical structures of OBO-ester (the OBO precursor) and OBO by ^1H and ^{13}C nuclear magnetic resonance spectroscopy, mass spectrometry, and elemental analysis are deposited in ESI† (Figures S1-5). Scheme 1 illustrates the chemical structure and reaction mechanism of OBO with Cd^{2+}.

OBD **OBO-Cd^{2+}**

Scheme 1 Reaction mechanism of OBO with Cd^{2+}.

The photophysical properties of OBO are assessed under physiological conditions (50 mM HEPES, 0.10 M KCl, pH 7.2). Figure 1 depicts the absorption spectra of OBO in the presence of various concentrations of Cd^{2+}. Free OBO exhibits two absorption bands at 304 nm ($\varepsilon = 3.82\times10^4$ $M^{-1}cm^{-1}$) and 380 nm ($\varepsilon = 5.82\times10^4$ $M^{-1}cm^{-1}$), corresponding to the π–π^* transition and ICT bands, respectively. Upon addition of Cd^{2+}, the π–π^* transition band decreases whereas the ICT band exhibits a hypsochromic shift to a new band at 354 nm ($\varepsilon = 7.18\times10^4$ M^{-1} cm^{-1}), accompanying with two isosbestic points at 313 and 370 nm. The ratio of absorbance at 354 to 405 nm (A_{354}/A_{405}) increases with the addition of Cd^{2+} concentrations (Figure S6 in ESI†), indicating the formation of complex between OBO and Cd^{2+}. Similar results were obtained by taking the ratio of absorbance at 354 to 380 nm. The formation of the OBO-Cd^{2+} complex is further confirmed by ^{1}H NMR spectra and the quantum chemical calculations. Herein, the choice of 405 nm is in line with the use of laser-induced excitation to capture the living cells image incorporating with OBO-ester and Cd^{2+} under the confocal fluorescent microscope (*vide infra*).

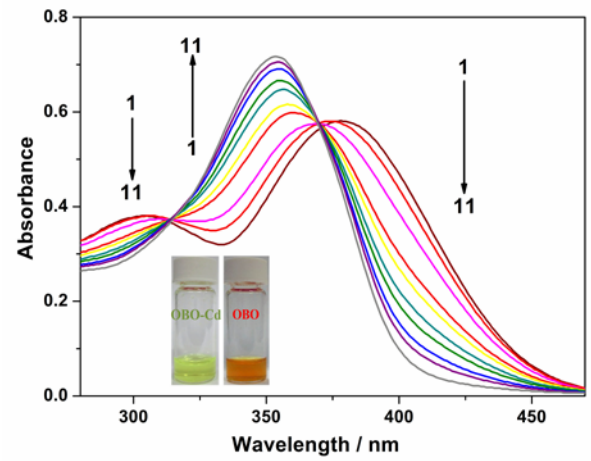

Figure 1. Absorption spectra of 10.0 μM OBO in 50 mM HEPES (pH 7.2) containing 0.10 M KCl with various concentrations (1–11: 0.0, 1.0, 2.0, 3.0, 4.0, 5.0, 6.0, 7.0, 8.0, 9.0, and 10.0 μM) of Cd^{2+} ion. The bottom inset displays images of OBO with (left) and without (right) Cd^{2+}.

The ^{1}H NMR spectrum of OBO-Cd^{2+} shows that the protons (H_a and H_b) in *N*-methylene of acetate and 3-position of benzene display the upfield shifts when OBO binds to Cd^{2+} (Figure S7 in ESI†), suggesting that the binding site is BAPTA. The quantum chemical calculation also supports this conclusion. Figure S8 (ESI†) depicts the optimal geometries of free OBO and OBO-Cd^{2+} complex which indicate the structure and the binding site at the BAPTA moiety of OBO. It clearly visualizes that the Cd^{2+} ion binds to the oxygen and nitrogen atoms of BAPTA. The main coordinated bond lengths at this binding site are summarised in Table S1 (ESI†). The main coordinated bond lengths of Cd-O1, Cd-O2, Cd-O3, and Cd-O4 are slightly shorter than the reported Cd-O bond length, suggesting a strong interaction between the tetra-carboxyl groups and Cd^{2+}. By contrast, the Cd-O5 and Cd-O6 bond lengths are longer and exceed the range of bond force, inferring that the phenoxyethane moieties have almost no interaction with Cd^{2+}. The Cd-N7 and Cd-N8 bond lengths are longer than the usual Cd-N bond length, inferring a weaker interaction between the N atoms and Cd^{2+}.[16] Tables S2 and S3 (ESI†) display the ground-state energies and Cartesian coordinates of OBO and OBO-Cd^{2+} complex in water at the B3LYP/LanL2DZ+6-31G* level. These results again corroborate the formation of OBO-Cd^{2+} complex with the binding site at BAPTA.

Figure 2 depicts the emission spectra of OBO on the addition of various concentrations of Cd^{2+} at an excitation wavelength of 405 nm. Free OBO exhibits an emission maximum (λ^{fl}_{max}) of 594 nm with an enormous Stokes shift of 189 nm. The quantum yield (φ) is 0.024. Upon addition of Cd^{2+}, the λ^{fl}_{max} undergoes a hypsochromic shift to 532 nm with an increase in fluorescence and the φ is 0.078. The inset displays the changes in emission intensities at 532 and 594 nm, respectively by plotting (F–F_o) against concentration of Cd^{2+}, where F and F_o are the emission intensities with and without Cd^{2+}, respectively. It is clearly seen that the emission intensities at 532 and 594 nm increase with the increase in the concentration of Cd^{2+}. A good linear relationship is observed between (F–F_o) and [Cd^{2+}] (0.0–0.40 μM). The detection limit is found to be 20 nM (3σ/slope), demonstrating that OBO is a highly sensitive probe for Cd^{2+}.

To gain further insight of the spectral properties, the quantum chemical calculations are conducted by the Gaussian 09 program. The geometric parameters of OBO and OBO-Cd^{2+} are optimised by the hybrid Becke three-parameter Lee-Yang-Parr exchange correlation functional (B3LYP) method[17] with LanL2DZ+6-31G* mixed basis set (LanL2DZ[18] for Cd and 6-31G* for other atoms). Figure S9 (ESI†) shows that the electrons of free OBO are localised on one side in HOMO and the ethoxyphenyl group does not participate in the rearrangement of electrons. A total electron transfer from one side to another is observed between the HOMO and LUMO. When OBO binds with Cd^{2+}, the BAPTA-Cd moiety is formed which functions as a bridge to connect the two OXO fluorophores. Electrons are localised on the whole molecule of the HOMO, making the π-conjugated system larger and preserving the ICT process. However, the calculated energy gap between the LUMO and HOMO of OBO-Cd^{2+} (3.171 eV) is larger than that of free OBO (2.567 eV). This is in agreement with the hypsochromic shift of the absorption and emission spectra of OBO upon the formation of an OBO-Cd^{2+} complex. In summary, the π-conjugated system could enhance the fluorescence intensity and the ICT spectrum of OBO is hypsochromically shifted upon complexation with Cd^{2+}.

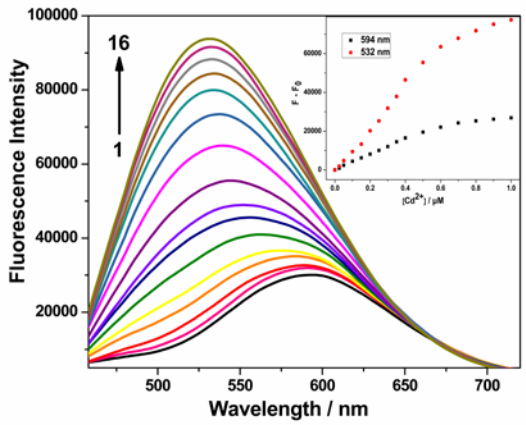

Figure 2. Fluorescence emission spectra of 1.0 μM OBO in 50 mM HEPES (pH 7.2) containing 0.10 M KCl with various concentrations (1–16: 0.0, 0.025, 0.05, 0.1, 0.15, 0.2, 0.25, 0.3, 0.35, 0.4, 0.5, 0.6, 0.7, 0.8, 0.9, and 1.0 μM) of Cd^{2+} at an excitation wavelength of 405 nm. The inset displays (F–F_o) against concentration of Cd^{2+}, where F and F_o are the fluorescent intensities at 532 and 594 nm with and without Cd^{2+}, respectively.

The stoichiometric ratio of OBO-Cd^{2+} complex is determined as 1:1 by the Job's method (Figure S10 in ESI†). The Hills plot is applied to determine the dissociation constant of OBO-Cd^{2+} complex as 116.0 ± 27.0 nM (Figure S11 in ESI†), suggesting the affinity of OBO to Cd^{2+} is much larger than other reported Cd^{2+} probes.[4,5b,6,12b] The fluorescence lifetimes of the free OBO and OBO-Cd^{2+} complex determined from time-resolved fluorescence spectroscopy are 1.41 and 1.48 ns at an excitation wavelength of 405 nm, respectively.

The fluorescence titration of OBO with various metal ions is depicted in Figure S12a (ESI†). Among these metal ions, OBO displays excellent selectivity to Cd^{2+} with a strong fluorescence enhancement while other bivalent metal ions exhibit slight fluorescence quenching on OBO. Most importantly, OBO has almost no response to Zn^{2+} and is thus superior to other Cd^{2+} probes which often suffer from Zn^{2+} interference.[13] In addition, the co-existence of other bivalent metal ions do not affect the measurement of Cd^{2+} (Figure S12b in ESI†), demonstrating that OBO possesses excellent selectivity to Cd^{2+} over other bivalent metal ions. Fluorescent pH titration in the biologically relevant pH range (5.5–9.0) shows that the optimal working pH of OBO or OBO-Cd^{2+} complex is 7.0 (Figure S13 in ESI†) which should meet their uses under physiological environment.

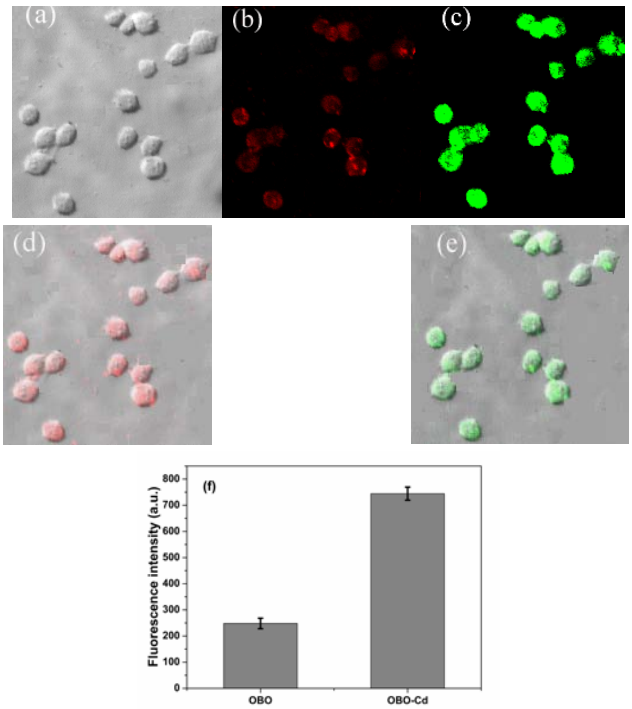

Figure 3. Confocal fluorescent images of MCF-7 cells stained with 5.0 μM OBO-ester at an excitation wavelength of 405 nm: (a) Bright field transmission image of MCF-7 cells incubated with OBO-ester. (b) Fluorescence image of MCF-7 cells incubated with OBO-ester at emission 570–610 nm. (c) Fluorescence image of MCF-7 cells incubated with OBO-ester for 30 min and then further incubated with 5.0 μM $CdCl_2$ for 30 min at emission 510–550 nm. (d) Images a and b are overlapped. (e) Images a and c are overlapped. (f) Comparison of the average intracellular fluorescence intensity with OBO at 570–610 nm and OBO-Cd^{2+} at 510–550 nm. Data are expressed as mean ± standard derivation of 10 cells.

In order to examine the ability of OBO to track the intracellular Cd^{2+} level, OBO-ester was employed for the cell permeability. MCF-7 cells were incubated with OBO-ester (5.0 μM) for 30 min at 37 °C, and then the ester was converted to the active form of OBO inside the cells by intracellular esterase, allowing the intracellular Cd^{2+} to be deciphered in the cytosol. Then exogenous Cd^{2+} was further introduced via incubation with 5.0 μM $CdCl_2$ for another 30 min. The images were recorded at 570–610 and 510–550 nm under the excitation wavelength of 405 nm (Figure 3b & c), respectively. Figure 3a depicts the bright field transmission image of the cells under the confocal microscope. Very clear cell image is observed. The cells turn to red after they have been exposed to OBO-ester, suggesting the penetration of OBO-ester into the cell. The cells are changed to bright green after they have been incorporated with Cd^{2+}, demonstrating that Cd^{2+} can permeate into the cells and bind with OBO to form OBO-Cd^{2+}. Figure 3d and e presents the fluorescence images of the MCF-7 incorporated with OBO-ester in the absence and presence of Cd^{2+}, respectively. It is clear that OBO can stain the cells and also indicate the presence of Cd^{2+}. Moreover, Figure 3f shows the mean fluorescent intensities of each cell captured at 570–610 and 510–550 nm, respectively. The emission intensity at 510–550 nm is about three times larger than that at 570–610 nm, corroborating that the emission intensity of OBO is enhanced in the presence of Cd^{2+} as shown in Figure 2. Our results demonstrate that OBO can be potentially useful for imaging Cd^{2+} in living cells under a confocal laser scanning microscope.

In summary, we have successfully designed an organic salt as a fluorescent probe for Cd^{2+} based on the ICT principle. This probe exhibits a large Stokes shift of 189 nm and a low detection limit of 20 nM Cd^{2+} under visible excitation. Moreover, its high sensitivity and selectivity to Cd^{2+} in aqueous environment facilitate the possible application of OBO in imaging Cd^{2+} in living cells, further demonstrating its potential for Cd^{2+} detection in biological systems.

This work is supported by the Hundred Talent Programme of Shanxi Province, and National Natural Science Foundation of China (21175086 and 21175087).

Notes and references

[a]*Institute of Environmental Science, and School of Chemistry and Chemical Engineering, Shanxi University, Taiyuan 030006, P. R. China. Fax: +86-351-7018613; Tel: +86-351-7018613; E-mail: dc@sxu.edu.cn*
[b]*Department of Chemistry, Taiyuan Normal University, Taiyuan 030031, P. R. China*
[c]*Department of Chemistry, Hong Kong Baptist University, 224 Waterloo Road, Kowloon Tong, Hong Kong SAR, P. R. China. Fax: +852-34117348; Tel: +852-34117839; E-mail: mfchoi@hkbu.edu.hk*

† Electronic Supplementary Information (ESI) available: Detailed synthetic procedures, supplementary figures, NMR spectra and mass spectrum. See DOI: 10.1039/b000000x/

1 (*a*) A. M. S. Mendes, G. P. Duda, C. W. A. do Nascimento and M. O. Silva, *Sci. Agric.*, 2006, **63**, 328-332; (*b*) L. Järup and A. Akesson, *Toxicol. Appl. Pharmacol.*, 2009, **238**, 201-208.
2 (*a*) C. C. Bridges and R. K. Zalups, *Toxicol. Appl. Pharmacol.*,2005**, 204,** 274-308; (*b*) B. J. Julin, A. Wolk, L. Bergkvist, M. Bottai and A. Akesson, *Cancer Res.*, 2012, **72**, 1459-1466.
3 (*a*) M. P. Waalkes, S. Rehm and C. W. Riggs, *Cancer Res.*, 1988, **48**, 4656-4663; (*b*) M. P. Waalkes, *Mutat. Res.*, 2003, **533**, 107-120.
4 T. Cheng, Y. Xu, S. Zhang, W. Zhu, X. Qian and L. Duan, *J. Am. Chem. Soc.*, 2008, **130**, 16160-16161.
5 (*a*) Z. Liu, C. Zhang, W. He, Z. Yang, X. Gao and Z. Guo, *Chem. Commun.*, 2010, **46**, 6138-6140; (*b*) Y. Tan, J. Gao, J. Yu, Z. Wang, Y. Cui, Y. Yang and G. Qian, *Dalton Trans.*, 2013, **42**, 11465-11470.
6 Z. Li, P. Xi, L. Huang, G. Xie, Y. Shi, H. Liu, M. Xu, F. Chen and Z. Zeng, *Inorg. Chem. Commun.*, 2011, **14**, 1241-1244.
7 W. -L. Gong, M. P. Aldred, G. -F. Zhang, C. Li and M. -Q. Zhu, *J. Mater. Chem. C*, 2013, **1**, 7519-7525.
8 A. Sahana, A. Banerjee, S. Lohar, S. Guha, S. Das, S. K. Mukhopadhyay and D. Das, *Analyst*, 2012, **137**, 3910-3913.
9 H. H. Lee, S. H. Jung, S. Park, K. M. Park and J. H. Jung, *New J. Chem.*, 2013, **37**, 2330-2335.
10 Y. Li, L. Li, X. Pu, G. Ma, E. Wang, J. Kong, Z. Liu and Y. Liu, *Bioorg. Med. Chem. Lett.*, 2012, **22**, 4014-4017.

11 (*a*) X. L. Tang, X. H. Peng, W. Dou, J. Mao, J. R. Zheng, W. W. Qin, W. S. Liu, J. Chang and X. J. Yao, *Org. Lett.*, 2008, **10**, 3653-3656; (*b*) G. M. Cockrell, G. Zhang, D. G. Van Derveer, R. P. Thummel and R. D. Hancock, *J. Am. Chem. Soc.*, 2008, **130**, 1420-1430.
12 (*a*) T. Cheng, T. Wang, W. Zhu, Y. Yang, B. Zeng, Y. Xu and X. Qian, *Chem. Commun.*, 2011, **47**, 3915-3917; (*b*) L. Xin, Y. Z. Chen, L.Y. Niu, L. Z. Wu, C. H. Tung, Q. X. Tong and Q. Z. Yang, *Org. Biomol. Chem.*, 2013, **11**, 3014-3019.
13 (*a*) X. Jiang, B. G. Park, J. A. Riddle, B. J. Zhang, M. Pink and D. Lee, *Chem. Commun*., 2008, 6028-6030; (*b*) K. M. K. Swamy, M. J. Kim, H. R. Jeon, J. Y. Jung and J. Yoon, *B. Korean Chem. Soc.*, 2010, **31**, 3611-3616.
14 G. C. Midya, S. Paladhi, S. Bhowmik, S. Saha and J. Dash, *Org. Biomol. Chem.*, 2013, **11,** 3057-3063.
15 X. Li, X. Gao, W. Shi and H. Ma, *Chem. Rev.*, 2013, DOI: 10.1021/cr300508p.
16 (*a*) B. J. Carra, S. M. Berry, R. D. Pike and D. C. Bebout, *Dalton Trans.* 2013**, 42**, 14424-14431; (*b*) W. Yuan, T. Liu, Z. Guo, H. Li and R. Cao, *J. Mol. Struct*., 2010, **965**, 82-88.
17 A. D. Becke, *J. Chem. Phys*., 1993, **98**, 5648-5653.
18 P. J. Hay and W. R. Wadt, *J. Chem. Phys.*, 1985, **82**, 270-283.

